First-principles determination of magnetic properties

2003 J. Phys.: Condens. Matter 15 S587

(http://iopscience.iop.org/0953-8984/15/5/312)

INSTITUTE OF PHYSICS PUBLISHING JOURNAL OF PHYSICS: CONDENSED MATTER

J. Phys.: Condens. Matter **15** (2003) S587–S598 PII: S0953-8984(03)55332-2

First-principles determination of magnetic properties

Ruqian Wu, Zongxian Yang and Jisang Hong

Department of Physics, University of California, Irvine, CA 92697-4575, USA

Received 29 October 2002
Published 27 January 2003
Online at stacks.iop.org/JPhysCM/15/S587

Abstract

First-principles density functional theory calculations have achieved great success in the exciting field of low-dimension magnetism, in explaining new phenomena observed in experiments as well as in predicting novel properties and materials. As known, spin–orbit coupling (SOC) plays an extremely important role in various magnetic properties such as magnetic anisotropy, magnetostriction, magneto-optical effects and spin-dynamics. Using the full potential linearized augmented plane wave approach, we have carried out extensive investigations for the effects of SOC in various materials. Results of selected examples, such as structure and magnetic properties of Ni/Cu(001), magnetism and magnetic anisotropy in magnetic Co/Cu(001) thin films, wires and clusters, magnetostriction in FeGa alloys and magneto-optical effects in Fe/Cr superlattices, are discussed.

1. Introduction

Magnetism in low dimensions is one of the most active areas nowadays due to demands from applications in high-density storage, communication and sensor technologies [1]. The alternation in local coordinates in magnetic surfaces, interfaces, wires and nano-clusters brings in abundant novel phenomena such as enhancements of magnetization, strong magnetic anisotropy, peculiar magnetic phase transitions, and more recently magneto-transport [2–4]. While significant progress has been made to understand and manipulate these properties, plenty of challenges still exist even at the fundamental level. Due to the complexities of most magnetic phenomena, strong interplay between theory and experiment is usually crucial to establish reliable physical pictures and trends.

As discussed in numerous important papers by Professor Baberschke [5], spin–orbit coupling (SOC) plays an essential role in magnetism. It is the only term in the Hamiltonian that links the spatial and spin parts of wavefunctions, and thus serves as the origin of many significant phenomena such as magnetic crystalline anisotropy (MCA), magnetostriction, magneto-optical Kerr effects (MOKE), magnetic circular dichroism (MCD) and magnetic damping. In most magnetic systems, however, the SOC contributions are very weak compared to those from crystalline fields and exchange interactions. One thus needs to be extremely

careful in treating SOC in magnetic transition metal systems [6]. Significant progress has been achieved in the last decade in improving numerical stability and reliability of the determination of SOC induced properties.

In this paper, we will discuss some of our recent results in low-dimension magnetism, especially those related to SOC. In the following, the methodology and background will be given in section 2; results of selected systems such as Ni/Cu(001), Co wire and clusters, FeGa alloys and Fe/Cr superlattices will be discussed in section 3. Final conclusions will be provided in section 4.

2. Methodology

2.1. FLAPW method

The thin-film version of the full potential linearized augmented plane wave (FLAPW) method [7] is employed in our calculations. Single-slab geometry is used to simulate surfaces and thin films. The real space is divided into three different regions, namely muffin-tin (MT) spheres around the nuclei, a vacuum region on each side of the slab and the remaining interstitial region. The augmented plane wave basis function is expanded in a 'natural' representation as

$$\phi_{k+G} = \begin{cases} \mathrm{e}^{\mathrm{i}(\vec{k}+\vec{G})\cdot\vec{r}}/\sqrt{\Omega} \\ \mathrm{e}^{\mathrm{i}(\vec{k}+\vec{G})\cdot\vec{R}_i} \sum_{l,m} \mathrm{i}^l [a^i_{lm} u_l(r) + b^i_{lm} \dot{u}_l(r)] Y_{lm}(\hat{r}) \\ \mathrm{e}^{\mathrm{i}(\vec{k}+\vec{G})_\parallel \cdot \vec{r}_\parallel} [a^V_{(\vec{k}+\vec{G})} u_{(\vec{k}+\vec{G})_\parallel}(z) + b^V_{(\vec{k}+\vec{G})} \dot{u}_{(\vec{k}+\vec{G})_\parallel}(z)] \end{cases} \tag{1}$$

where $\vec{k}$ and $\vec{G}$ are wave-and lattice vectors, Ω is the volume of the unit cell, $\vec{R}_i$ is the position of the ith atom, $u_l(r)$ is the solution of the radial semi-relativistic Kohn–Sham equation for angular momentum number l in this MT region and $\dot{u}_l(r)$ is its energy derivative. Similarly, $u_{(\vec{k}+\vec{G})_\parallel}(z)$ and $\dot{u}_{(\vec{k}+\vec{G})_\parallel}(z)$ are the solution and its energy derivative of the one-dimensional Kohn–Sham equation in the vacuum region. The matching coefficients, a and b, ensure the continuity of each basis function and its first derivative across MT and vacuum boundaries [7].

'Natural' expansions are also applied to charge densities and potentials. Obviously, no shape approximation is introduced in FLAPW expansions and the adjustable semi-relativistic basis function allows a maximum possible flexibility to accommodate even tiny changes in the MT region. The FLAPW method is known as one of the most accurate and powerful first principles quantum mechanical simulation packages based on the density functional theory. In practical calculations, we use $l_{max} = 8$ for expansions of wavefunction, charge and potential in the MT region. Convergences of results with respect to the completeness of basis set and number of sampling k-points are checked.

2.2. SOC Hamiltonian

As known, SOC is the only term in the Hamiltonian that links the spin space and real space and thus is the origin of magneto-crystalline anisotropy and magneto-optical effects. In a central potential $V(r)$, the SOC Hamiltonian, H^{SOC}, is given as

$$H^{SOC} = \xi \hat{\sigma} \cdot \hat{l} \qquad \text{and} \qquad \xi = \frac{1}{4m^2c^2} \frac{1}{r} \frac{\mathrm{d}V}{\mathrm{d}r}. \tag{2}$$

This format however has been successfully generalized to almost all cases since the major contribution is clearly from the near nuclear region where the $\mathrm{d}V/\mathrm{d}r$ term is large and the spherical symmetry is retained. In addition, the value of ξ is a few tens of millielectron

volts in most 3d metals, much smaller than their crystalline fields. Therefore, H^{SOC} can be conveniently treated in a second variational approach, based on the ground state properties obtained from semi-relativistic calculations [8].

In numerical calculations, one needs to construct the SOC matrix

$$\hat{\sigma}\cdot\hat{l} = \begin{pmatrix} \uparrow\uparrow & \uparrow\downarrow \\ \downarrow\uparrow & \downarrow\downarrow \end{pmatrix} = \begin{pmatrix} \frac{A_+ + A_-}{2}\sin\theta + L_z\cos\theta & (A_-\cos^2\frac{\theta}{2} - A_+\sin^2\frac{\theta}{2} - L_z\sin\theta)\mathrm{e}^{-\mathrm{i}\phi} \\ (A_+\cos^2\frac{\theta}{2} - A_-\sin^2\frac{\theta}{2} - L_z\sin\theta)\mathrm{e}^{\mathrm{i}\phi} & -\frac{A_+ + A_-}{2}\sin\theta - L_z\cos\theta \end{pmatrix} \quad (3)$$

where θ and ϕ stand for the polar and azimuthal angles of the magnetic moment and $A_+ = \mathrm{e}^{-\mathrm{i}\phi}(L_x + \mathrm{i}L_y)$ and $A_- = \mathrm{e}^{\mathrm{i}\phi}(L_x - \mathrm{i}L_y)$. After re-diagonalizing the $N_e \times N_e$ eigenvalue problem,

$$\begin{pmatrix} \varepsilon_i\uparrow & 0 \\ 0 & \varepsilon_i\downarrow \end{pmatrix} + \xi\hat{\sigma}\cdot\hat{l} = \varepsilon' I \quad (4)$$

the wavefunction, charge density, potential, energy band and total energy will be updated and become (θ, ϕ) dependent. Here $N_e = N_e\uparrow + N_e\downarrow$ is the number of states invoked in the variational procedure, and $\varepsilon_i\uparrow(\varepsilon_i\downarrow)$ are the eigenenergies in the majority (minority) spin channels, respectively. It has been shown that SOC alters charge density, spin density and spin moment negligibly in most 3d transition metal systems and it is thus not important to treat H^{SOC} self-consistently there [6].

2.3. Determination of magnetic anisotropy and magnetostriction

Magnetic anisotropy is one of the most important phenomena in low-dimension magnetism and has attracted extensive attention in the last decade. It is important in various aspects of applications such as thermal stability, coercivity and perpendicular magnetic recoding; and challenges for fundamental understanding. There are three approaches currently to calculate E_{MCA}, namely, the force theorem [9, 10], total energy [11] and torque [12]. It can be shown that they produce very close results for most 3d systems in converged calculations [6, 11].

The force theorem assumes that the contribution from the SOC-induced change in charge density, $\Delta\rho$, is negligible in total energy and thus E_{MCA} can be evaluated merely from the SOC-induced changes in eigenvalues as

$$E_{MCA} = \sum_{occ'} \varepsilon_i'(\theta_1, \phi_1) - \sum_{occ''} \varepsilon_i''(\theta_2, \phi_2) + \mathrm{O}(\Delta\rho^n). \quad (5)$$

The main disadvantage of the force theorem is in the determination of the sets of occupied states (i.e., occ$'$ and occ$''$). If one simply uses the Fermi filling, large contributions may arise from the near-degenerate states (or even may have no relevance at all with SOC). State tracking [13], Gauss broadening and an enormous number of k-points [14] are needed in these situations.

A large number of k-points are also needed to calculate E_{MCA} from the total energies. In addition, a much higher level of charge or potential convergence is needed to obtain the tiny E_{MCA} from two very large numbers.

The torque method gives stable results with many fewer k-points since it evaluates E_{MCA} through the expectation values of the angular derivative of H^{SOC} at a magic angle (θ_m, ϕ_m)

$$E_{MCA} = \sum_{occ} \langle\Psi_i'(\theta_m, \phi_m)|\frac{\partial H^{SOC}}{\partial\theta}|\Psi_i'(\theta_m, \phi_m)\rangle. \quad (6)$$

The magic angle (θ_m, ϕ_m) can be found from the symmetry, or more explicitly the form of angular dependence of total energy. For a uniaxial system, where $E = E_0 + k_2 \sin^2\theta + k_4 \sin^4\theta$, it can be proven that $\theta_m = 45°$ and $\phi_m = 0°$.

In most magnetic thin films, large uniaxial magnetic anisotropy energies are induced not only by the surface and interface effects but also by lattice strains due to lattice mismatches [15]. The surface and interface contributions also sensitively depend on the atomic relaxations [16]. It is thus important to determine the magnetostriction coefficient in different scenarios [17, 18]. Through analyses, one can find that the magnetostrictive coefficient of a given system can be determined from the strain dependences of its E_{MCA} and total energy, E, as

$$\lambda = \alpha \frac{\Delta l}{l} = \frac{\alpha}{l} \frac{\mathrm{d}E_{MCA}/\mathrm{d}l}{\mathrm{d}^2E/\mathrm{d}l^2} \tag{7}$$

where α is a coefficient (=3/2 for cubic systems, when λ is labelled as λ_{001} or λ_{111}) [19, 20].

2.4. Determination of magneto-optical Kerr effect and magnetic circular dichroism

The components of the optical conductivity tensor, $\hat{\sigma}$, are given by a sum of inter-band and intra-band contributions. Within the random phase approximation (RPA), the inter-band part of $\hat{\sigma}$ is calculated by means of the linear-response formula [21, 22]

$$\sigma_{\alpha\beta} = \frac{\mathrm{i}e^2}{m^2\hbar\Omega} \sum_{k,m,n} \frac{f_m - f_n}{\omega_{mn}} \frac{P^{\alpha}_{nm} P^{\beta}_{mn}}{\omega - \omega_{mn} - \mathrm{i}\delta} \tag{8}$$

where $f_{m,n}$ is the Fermi occupation factor, $\omega_{mn} = \varepsilon_m - \varepsilon_n$ is the energy difference, δ is a lifetime broadening parameter and $P^{\alpha,\beta}_{mn}$ are matrix elements of the momentum operator. The intra-band contribution to the diagonal components of the conductivity is normally calculated according to the Drude formula with two material dependent parameters (σ_0 and τ),

$$\sigma_D = \frac{\sigma_0}{1 - \mathrm{i}\omega\tau}. \tag{9}$$

The complex magneto-optical Kerr rotation angle can then be calculated

$$\Phi = -\frac{\sigma_{xy}}{\sigma_{xx}} \sqrt{1 + \frac{\mathrm{i}4\pi\sigma_{xx}}{\omega}}. \tag{10}$$

A very similar linear-response formula as in equation (8) can be used to calculate the MCD and x-ray adsorption spectroscopy. In this case, it is more convenient to use matrix elements $P^{\pm}_{cv}$ between valence and core states [23].

3. Examples of results

First-principles calculations based on the density functional theory [24] have played a major role during the renaissance of magnetism by predicting new magnetic properties and materials, as well as by providing unprecedented insights for explanation of experimental data. Several examples discussed here demonstrate that accurate results can be obtained for a wide spectrum of properties such as atomic structures, spin and orbital magnetic moments, magnetic ordering and magnetic anisotropy energies, magnetostrictive coefficients and magneto-optical response functions.

Table 1. Calculated vertical atomic positions, z (in au), magnetic moments, $\langle S_z \rangle$ and $\langle L_z \rangle$ (in μ_B) for the Ni/Cu systems.

Quantity	Cu(I)	Ni	Ni	Ni	Ni	Cu	Cu	Co
Ni_4/Cu(001)								
z	6.99	10.44	13.71	17.05	20.11			
$\langle S_z \rangle$	−0.005	0.46	0.65	0.69	0.74			
$\langle L_z \rangle$	0.0	0.043	0.054	0.062	0.068			
Cu_2/Ni_4/Cu(001)								
z	6.99	10.44	13.65	16.88	20.09	23.57	27.00	
$\langle S_z \rangle$	−0.006	0.47	0.66	0.66	0.48	−0.001	−0.003	
$\langle L_z \rangle$		0.043	0.054	0.054	0.044			
Co/Cu_2/Ni_4/Cu(001)								
z	6.99	10.44	13.65	16.88	20.11	23.50	27.03	30.39
$\langle S_z \rangle$	−0.007	0.48	0.67	0.67	0.47	−0.017	−0.020	1.92
$\langle L_z \rangle$		0.042	0.054	0.055	0.041			0.12
NiCu/Ni_3/Cu(001)								
z	7.08	10.50	13.69	16.91	19.97			
					20.17(Cu)			
$\langle S_z \rangle$	−0.006	0.46	0.64	0.62	0.47			
$\langle L_z \rangle$		0.040	0.052	0.054	0.080			
Ni_3/NiCu/Cu(001)								
z	7.08	10.47	13.66	16.88	19.98			
		10.42(Cu)						
$\langle S_z \rangle$	−0.006	0.19	0.53	0.66	0.74			
$\langle L_z \rangle$		0.020	0.043	0.061	0.069			

3.1. Structure and magnetism of Ni films on Cu(001)

Ni/Cu(001) films have been extensively studied, mainly due to the unique spin reorientation transition as a function of film thickness [25–27]. The main issues involved are

(1) lattice strains in Ni films and Ni/Cu interfaces,
(2) spin and orbital magnetic moments of each Ni atom,
(3) possible Cu/Ni mixing in surface and interface layers and
(4) the thickness dependence of E_{MCA} and the explanation.

Very recently, atomic structures of the ultra-thin Ni_n/Cu(001) films were studied quantitatively by Platow *et al* [28] through fitting the LEED I–V (intensity versus electron beam voltage) curves. In contrast to some earlier work [29], they found that Ni grows pseudomorphically on Cu(001), and the Ni–Ni interlayer distances are almost independent of both film thickness and depth ($d_{\mathrm{Ni-Ni}}$ is about 5% smaller than $d_{\mathrm{Cu-Cu}}$ in bulk Cu). Furthermore, no structure change occurs when the Ni films undergo magnetic orientation transitions.

Using the FLAPW approach, we optimized the atomic structures of Ni_4/Cu(001), Cu_2/Ni_4/Cu(001), NiCu/Cu(001), Ni_3/NiCu/Cu(001) and NiCu/Ni_3/Cu(001) [30]. Overall, as listed in table 1, the average $d_{\mathrm{Ni-Ni}}$ is 3.23 au in all systems with sharp interfaces. This suggests a 5.4% contraction in $d_{\mathrm{Ni-Ni}}$ compared to $d_{\mathrm{Cu-Cu}}$ (3.41 au) in bulk Cu: a result that agrees excellently with experiments. Nevertheless, calculated $d_{\mathrm{Ni-Ni}}$ varies from surface to interface, while it is more uniform in LEED results [28].

The mixing of Cu and Ni in the interfacial area strongly diminishes the magnetization of Ni atoms. It was found that NiCu/Cu(001) is 'magnetically dead', and the magnetic moment

Table 2. Calculated spin and orbital magnetic moments (in μ_B) and magnetic anisotropy energy (in meV per Co atom) of Co and Co/Cu systems.

System	$\langle S_z \rangle$	$\langle L_z \rangle$	E_{MCA}
Co ML	2.11	0.12	−1.46
Co/Cu(001)	1.92	0.12	−0.61
Cu/Co/Cu(001)	1.74	0.12	+0.54
Co chain (3 × 1)	2.22	0.26	+1.15
Co chain (5 × 1)	2.23	0.28	+1.29
Co/Cu(001) (3 × 1)	1.91	0.15	+0.35
Co/Cu(001) (5 × 1)	1.92	0.15	+0.39
Co_2	2.06	0.22	+0.21
Co_3	1.97	0.16	+0.36
Co_4 (square)	2.22	0.26	+0.68
Co_6 (octahedron)	2.10	0.13	∼0.03

for the Ni atom in the mixed layer is reduced significantly, to 0.19 μ_B in Ni_3/NiCu/Cu(001) and 0.57 μ_B in NiCu/Ni_3/Cu(001). Interestingly, NiCu/Ni_3/Cu(001) is lower in energy by 0.46 eV/cell compared to Ni_3/NiCu/Cu(001). Therefore the 'floating surface alloying' is energetically preferred over 'interface mixing'. Experimentally, conflicting reports can be found [27–29, 31]; more recent experimental results of surface magnetic moment enhancement appear to rule out the possibility of a 'floating Cu' layer [27].

The large lattice strain was found to be responsible for the magnetic reorientation transition. Calculations done by us and also by the groups of Eriksson and Weinberger found that the strain-induced E_{MCA} is as large as 60–90 μeV/atom in bulklike Ni [18, 32, 33]. As discussed by Professor Baberschke [5], this bulk anisotropy can overcome the negative surface/interface contributions and lead to perpendicular magnetic anisotropy when the Ni film is thicker than 7–8 layers.

3.2. Magnetic anisotropy in thin films, wires and clusters

The magnetic anisotropy energies of a large number of magnetic thin films have been calculated with various different density functional approaches in the last decade [6]. It is believed that a well converged calculation can obtain highly reliable uniaxial E_{MCA} with accuracy better than 0.05 meV [34]. More importantly, the behaviour of MCA for transition metal thin films can now be related to more fundamental properties such as band structures and wavefunctions. This enables us to explore the underlying physics and, furthermore, to figure out a way to tune the MCA for transition metal systems. We will focus on discussing results of E_{MCA} for a prototype series of magnetic thin films: Co on Cu(001).

As listed in table 2, the calculated E_{MCA} for the free Co monolayer is −1.46 meV/atom, which indicates that it prefers in-plane magnetization. We found that this is due to the large pocket of negative E_{MCA} contributions around the $\bar{M}$ point. Detailed analyses revealed that the SOC interaction between a pair of states, the occupied $d_{xz,yz}$ and the unoccupied d_{z^2} in the minority spin channel, is responsible. One thus can tailor E_{MCA} of a Co monolayer by manipulating the energy position of the Co $d_{xz,yz}$ states. For example, hybridization with Cu 3d states in Co/Cu(001) and Cu/Co/Cu(001) effectively lowers the Co $d_{xz,yz}$ states by 1.0–1.5 eV in energy. As a result, E_{MCA} becomes −0.64 meV per Co atom in Co/Cu(001) and +0.54 meV per Co atom in Cu/Co/Cu(001), respectively.

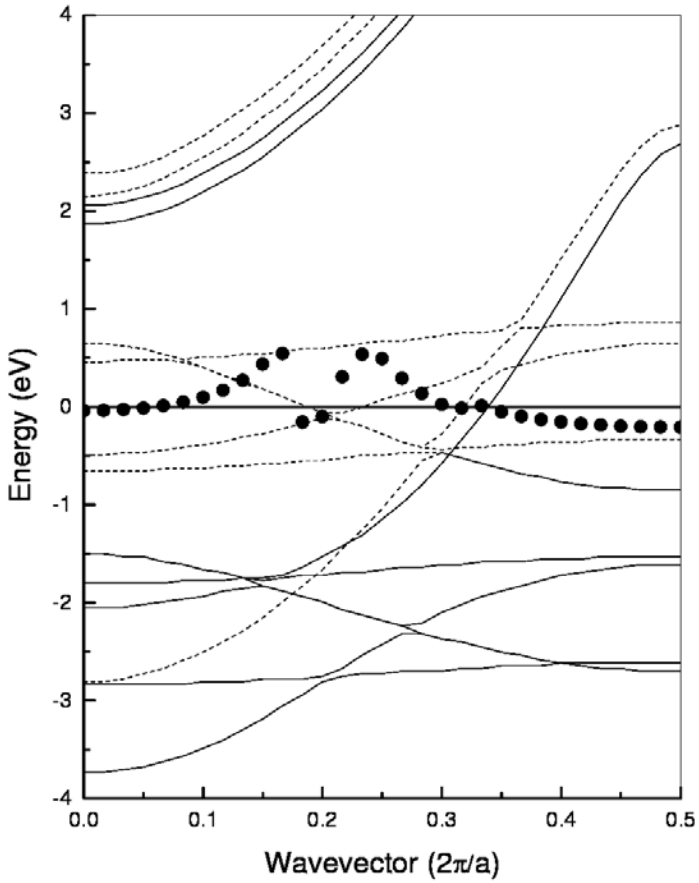

Figure 1. Calculated band structure (thin solid curves) and E_{MCA} (solid circles, due to contributions of the minority spin states only) distribution along the one-dimensional Brillouin zone for a free Co wire.

Very recently, we investigated magnetic Co wires on[1] Cu(001). To reduce and monitor interaction between adjacent wires, we used (1 × 3) and (1 × 5) unit cells in the lateral plane. First of all, the (1 × 3) and (1 × 5) cells give very close results as shown in table 2, indicating that the distance between adjacent wires (14.5–24.2 au) is reasonably large. The calculated values of E_{MCA} are positive, which means that the easy axis of a free Co wire is along the perpendicular direction. From the distribution of E_{MCA} along k_x (the Co chain aligns along the x-axis) in figure 1, one can find an obvious correlation between E_{MCA} and the occupancies of a pair of states ($d_{x^2-y^2}$ and d_{xy}) in the minority spin channel (dashed curves). They are separated by the Fermi level and make large positive E_{MCA} in the first 60% of the one-dimensional Brillouin zone. When both of them are occupied around $k_x = 0.2(2\pi/a)$, E_{MCA} dips to the negative region.

The calculated spin and orbital moments ($\langle S_z \rangle = 2.23\ \mu_B$ and $\langle L_z \rangle = 0.26\ \mu_B$, respectively) in a free Co wire are significantly enhanced compared to the corresponding values in a free Co monolayer (for $a = 4.83$ au, for example, $\langle S_z \rangle = 2.11\ \mu_B$ and $\langle L_z \rangle = 0.12\ \mu_B$, respectively). On Cu(001), they are reduced to $\langle S_z \rangle = 1.92\ \mu_B$ and $\langle L_z \rangle = 0.15\ \mu_B$, due to

[1] The Cu(001) substrate is simulated by a five-layer slab.

the proximity effects of Cu. It is important to note that the easy axis now turns to be along the chain on Cu(001); the energy difference between orientations along x (in-plane, along the chain) and y (in-plane, perpendicular to the chain) is also very small ($\sim$0.12 meV per Co atom).

Magnetic nano-clusters are receiving more attention for high-density magnetic recording media. E_{MCA} is a very important quantity for understanding and tailoring the thermal stability, coercivity and damping parameters. We have studied several smallest magnetic clusters, namely Co_2, Co_3, Co_4, Co_5 and Co_6. Results of selected systems are also given in table 2. Even with much shortened bond lengths (e.g., $d_{Co-Co} = 4.08$ au in the dimer), the Co magnetic moments are still very large. Unlike the Co monolayer, the easy axes of Co clusters are perpendicular to the Co–Co bonds in all cases. The magnitude of E_{MCA} is of the same order as in Co monolayers and wires, smaller than expected. For Co_4 in squares and Co_6 in octahedra, significant high order E_{MCA} contributions (i.e., the energy difference between magnetic orientations of $\phi = 0°$ and 45°) are obtained, 10–30 μeV per Co atom.

3.3. Magnetostriction in $Fe_{1-x}Ga_x$

Magnetostrictive materials are widely used in various sensor and actuator applications. Large magnetostriction is usually found in rare-earth/transition metal compounds [19], whereas most magnetic transition metal crystals and alloys show weak magneto-elastic effect. Very recently, it was found that the magnetostriction of bcc Fe is greatly enhanced by the addition of Ga [35, 36]. Room-temperature magnetostriction (λ_{001}) of $Fe_{1-x}Ga_x$, depending on x and also the quenching condition, can reach >200 ppm (10^{-6}), a value which corresponds to a tenfold increase above the magnetostriction of the pure bcc bulk Fe ($\lambda_{001} \approx 20$ ppm, $\lambda_{111} \approx -16$ ppm). This unusual enhancement challenges theoretical explanation [37].

While the structural phase diagram for $Fe_{1-x}Ga_x$ is rather complicated, it is instructive to start with three basic simple structures for $x = 0.25$, namely, DO_3, B2-like (or $L6_0$) and $L1_2$. To determine magnetostrictive coefficients, lattice strain along the z-axis (c/c_0) is used as a parameter[2]. The calculated results of E_{MCA} are plotted in figure 2. Interestingly, the calculated slopes of E_{MCA} (or equivalently the sign of λ_{001}) for the $L1_2$ and DO_3 structures are negative, while dE_{MCA}/dl is positive for the B_2-like structure. Quantitatively, the calculated values of λ_{001} are -107 ppm (10^{-6}), -298 ppm and +380 ppm for the DO_3, $L1_2$ and B_2-like structures, respectively. Overall, the magnitudes of λ_{001} for all these three structures are much larger than that for the pure bcc bulk Fe (20 ppm), owing to the stronger magneto-elastic coupling as well as to the smaller Young modulus. Experimentally, λ_{001} for $Fe_{1-x}Ga_x$ is +150 to +200 ppm, when x is 0.25. This indicates that the local B_2-like structure plays a key role for the strong positive magnetostriction in FeGa alloys.

The change in sign of λ_{001} from the DO_3 structure to the B_2-like structure is fascinating, since only the second-neighbour arrangement is altered. The calculated magnetic moments in the B_2-like structure (2.48 μ_B for Fe(1) in the mixed layer, 2.08 μ_B for Fe(2) in the pure layer and -0.08 μ_B for Ga) are very close to those in the DO_3 structure (2.41 μ_B for Fe(1), 1.96 μ_B for Fe(2) and -0.07 μ_B for Ga). The difference originates from very subtle changes in their band structures. In the DO_3 structure, the negative magnetostriction is associated with the strain dependence of the Fermi surface of the Fe(2) $d_{xz,yz}$ states, that couple with d_{z^2} and d_{xy,x^2-y^2} states. For the B_2-like structure, the Fe(2) $d_{xz,yz}$ states in the minority spin band become non-degenerate because of lower symmetry. Since they have the same magnetic quantum numbers (± 1), the SOC interaction between them leads to a positive magnetostriction.

[2] For the $L1_2$ and DO_3 structures, the constant volume mode was adopted in lattice distortion. For the $L6_0$-like structure, however, the lattice size in the x, y-plane was fixed (i.e., constant area mode) for the determination of elastic constants c_{11} and c_{12}.

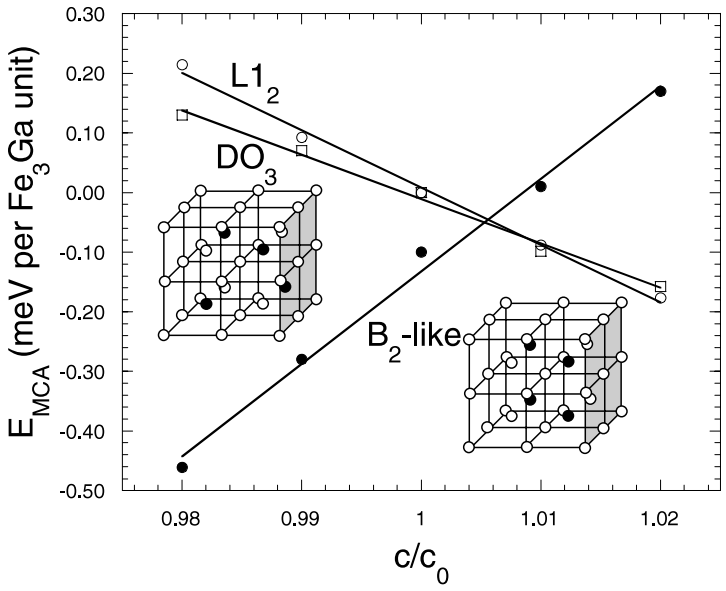

Figure 2. Calculated strain-induced magneto-crystalline anisotropy energies of Fe_3Ga. The DO_3 and Be-like structures are shown as insets, where the open circles represent Fe and the solid circles represent Ga.

The B2-like structure in the small cell is unfortunately unstable under tetragonal distortion and one thus needs to consider more complex geometries. Our recent calculations found that the B2-like structure can be stabilized either by mixing with the DO_3 structure or by removing some Ga atoms from the lattice. For the latter case, large magnetostrictive coefficient, +188 ppm, is found for the $Fe_{0.81}Ga_{0.19}$ alloy in the B2-like structure (by substituting one Ga atom with Fe in a 16-atom unit cell).

3.4. Magneto-optics in Fe/Cr(001) superlattices

The discovery of giant magnetoresistance has stimulated extensive studies on Fe/Cr superlattices in the last decade [38–40]. Depending on the thickness of the intervening Cr layers, the adjacent Fe films order either ferromagnetically (FM), antiferromagnetically (AFM) or even non-collinearly [41–43], that results in an alternation in the scattering condition for electron transport and thus the magnetoresistance. The change in magnetic ordering is expected to alter the optical and magneto-optical properties as well. MOKE was widely used as an *in situ* technique to monitor the FM/AFM phase transition [44]. Recently, magnetic-field-induced alternations in the infrared (IR) transmission and reflectance from the AFM Fe/Cr/Fe trilayers were also reported [45]. These optical properties, especially in the IR region, have been rarely studied so far.

We used a 20-layer slab ($Fe_5Cr_5Fe_5Cr_5$) to simulate the Fe/Cr superlattice and studied its MOKE and other optical properties. The atomic geometries are optimized through the atomic forces. Small but noticeable changes in the inter-layer distances are found in the interfacial regions when the magnetic phase transition occurs, which have not been considered in most previous calculations. The calculated total energy of the FM state is lower than that of the AFM state by $\Delta E = 6.9$ mRyd, which indicates that the FM state is the preferable phase in the ground state. This result agrees well with the findings of experimental observations at this thickness [40].

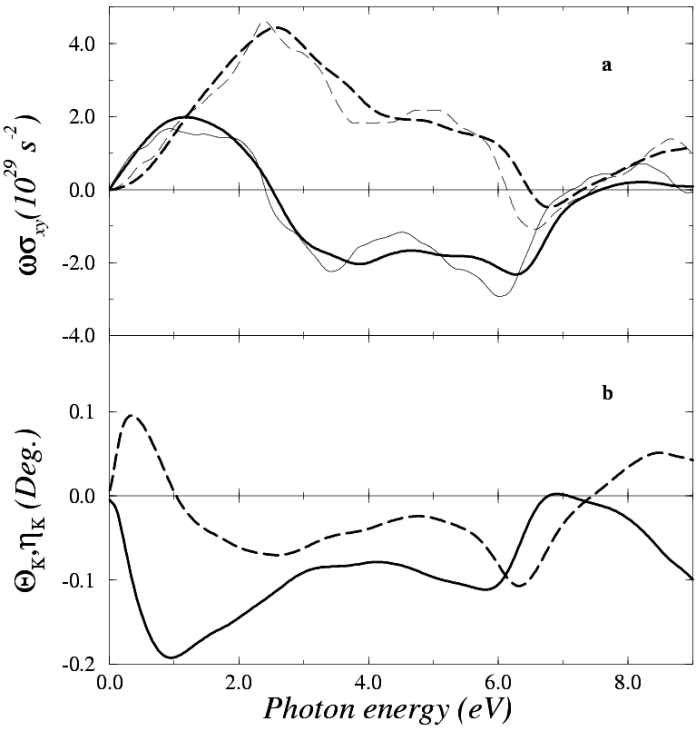

Figure 3. (a) Calculated spectra of real (solid curve) and imaginary (dashed curve) off-diagonal components of the conductivity accompanied by corresponding results of bulk Fe (thin curves); (b) Kerr rotation angle θ_K (solid curve) and Kerr ellipticity η_K (dashed curve) of Fe/Cr ferromagnetic superlattice.

In figure 3(a), the calculated spectra of $\omega\sigma_{xy}$ of Fe/Cr (thick curves) are very close to the results of bulk Fe (thin curves). In fact, the Cr contribution to σ_{xy} is cancelled completely in the FM Fe/Cr superlattice, owning to the anti-parallel alignment of their magnetic moments. On the other hand, Cr contributes to σ_{xx}. As a result, calculated MOKE spectra for the FM Fe/Cr superlattice in figure 3(b) also exhibit two pronounced peaks, in both the IR and in the near-ultraviolet regions around 6.0 eV; similar to bulk Fe but the magnitude is somewhat weaker (by a factor of two to three).

Our results show that magnetic ordering strongly modifies the optical spectra of n and k. This has been observed recently by Uran *et al* [45]; a small magnetic field is found to induce noticeable changes in the IR transmission of a Fe/Cr/Fe trilayer. The maximum in the change of reflectance and transmittance is found to occur near 2000 cm^{-1}. In figure 4 the relative changes[3] in reflectance, R, and transmittance, T, are presented. The calculated $\Delta R/R$ spectrum indeed has a pronounced maximum. Without the Drude term the maximum is near 2800 cm^{-1}. The Drude term is crucial to produce the sign change of $\Delta T/T$ and $\Delta R/R$ at the low-frequency end.

4. Conclusions

From the examples discussed above, it is obvious that high-quality first-principles density functional calculations can produce accurate results for a wide spectrum of magnetic properties of low-dimensional systems. Careful treatment of SOC is essential for the determination

[3] $\Delta R/R = 2[R(\mathrm{FM}) - R(\mathrm{AFM})]/[R(\mathrm{FM}) + R(\mathrm{AFM})]$ and $\Delta T/T = 2[T(\mathrm{FM}) - T(\mathrm{AFM})]/[T(\mathrm{FM}) + T(\mathrm{AFM})]$.

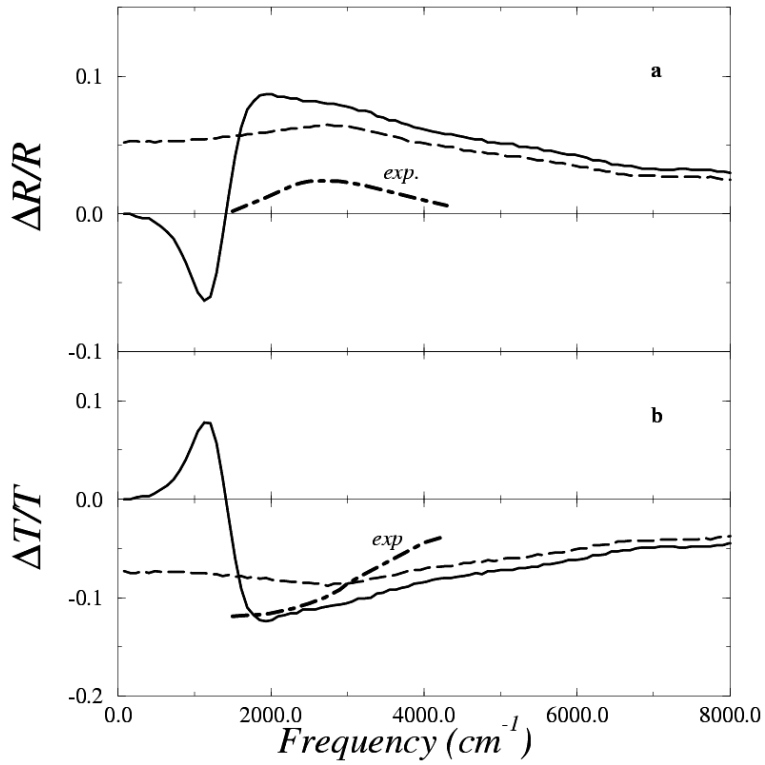

Figure 4. Calculated spectra of the relative changes of (a) reflectance and (b) transmittance of Fe/Cr superlattice. Solid and dashed curves represent results with and without the Drude intra-band contributions. Experimental results are reproduced with tenfold enhancement.

of magnetic anisotropy, magnetostriction and magneto-optical effects. It is expected that, through active collaborations with experimentalists, first-principles theory will play a more important role in the near future with rapid developments in computer hardware as well as in new algorithms and codes. Short-term challenges include new reliable approaches to treat non-equilibrium phenomena such as transport and damping.

Acknowledgments

We would like to thank Drs V G Gavrilenko, A J Freeman, A E Clark and K B Hathaway for stimulating discussions and collaborations. This work was supported by ONR (grant no N00014-95-1-0489) and by computing grants from NAVO, ARSC and ERDC.

References

[1] Cf
Freeman A J and Bader S D 1999 *Magnetism Beyond 2000* (Amsterdam: Elsevier)
[2] Baberschke K, Donath M and Nolting W 2001 *Band-Ferromagnetism* (Berlin: Springer)
[3] Freeman A J and Wu R Q 1991 *J. Magn. Magn. Mater.* **100** 497
[4] Prinz G A 1999 *J. Magn. Magn. Mater.* **200** 57
[5] See
Baberschke K 2001 Anisotropy in magnetism *Band-Ferromagnetism* ed K Baberschke, M Donath and W Nolting (Berlin: Springer)

[6] See review article
Wu R Q and Freeman A J 1999 *J. Magn. Magn. Mater.* **200** 498
[7] Wimmer E, Krakauer H, Weinert M and Freeman A J 1981 *Phys. Rev.* B **24** 864
Weinert M, Wimmer E and Freeman A J 1982 *Phys. Rev.* B **26** 4571
Weinert M 1981 *J. Math. Phys.* **22** 2433
[8] Koelling D D and Harmon B N 1977 *J. Phys. C: Solid State Phys.* **10** 3107
[9] Daalderop G H O, Kelly P J and Schuurmans M F H 1990 *Phys. Rev.* B **42** 1533
[10] Wang X D, Wang D S, Wu R Q and Freeman A J 1996 *J. Magn. Magn. Mater.* **159** 337
[11] Eriksson O 2001 *Band-Ferromagnetism* ed K Baberschke, M Donath and W Nolting (Berlin: Springer)
[12] Wang X D, Wu R Q, Wang D S and Freeman A J 1996 *Phys. Rev.* B **54** 61
[13] Wang D S, Wu R Q and Freeman A J 1993 *Phys. Rev. Lett.* **70** 869
Wang D S, Wu R Q and Freeman A J 1993 *Phys. Rev. Lett.* **71** 2166
[14] Gay J G and Richter R 1986 *Phys. Rev. Lett.* **56** 2728
[15] Baberschke K 1996 *Appl. Phys.* A **62** 417
[16] Wu R Q and Freeman A J 1996 *J. Appl. Phys.* **79** 6500
[17] Chen L J, Wu R Q and Freeman A J 1997 *J. Appl. Phys.* **81** 4417
[18] Hjorstam O, Baberschke K, Wills J M, Johansson B and Eriksson O 1997 *Phys. Rev.* B **55** 15026
James P, Eriksson O, Hjortstam O, Johansson B and Nordstrom L 2000 *Appl. Phys. Lett.* **76** 915
[19] Clark A E and Hathaway K B 2000 *Handbook of Giant Magnetostrictive Materials* ed G Engdahl (London: Academic)
[20] Wu R Q 2001 *Band-Ferromagnetism* ed K Baberschke, M Donath and W Nolting (Berlin: Springer)
[21] Wang C S and Callaway J 1974 *Phys. Rev.* B **9** 4897
[22] Oppeneer P M, Maurer T, Sticht J and Kübler J 1992 *Phys. Rev.* B **45** 10924
[23] Wu R Q, Wang D S and Freeman A J 1994 *J. Magn. Magn. Mater.* **132** 103
[24] Hohenberg P and Kohn W 1964 *Phys. Rev.* B **136** 864
Kohn W and Sham L J 1965 *Phys. Rev.* A **140** 1133
[25] Schulz B and Baberschke K 1994 *Phys. Rev.* B **50** 13467
[26] Farle M, Platow W, Anisimov A N, Poulopoulos P and Babersche K 1997 *Phys. Rev.* B **56** 5100
[27] Ney A, Scherz A, Poulopoulos P, Lenz K, Wende H, Babersche K, Wilhelm F and Brooks N B 2002 *Phys. Rev.* B **65** 024411
[28] Platow W, Bovensiepen U, Poulopoulos P, Farle M, Baberschke K, Hammer L, Walter S, Muüller S and Heinz K 1999 *Phys. Rev.* B **59** 12641
[29] Kim S H, Lee K S, Min H G, Jikeun Seo, Hong S C, Rho T H and Kim Jae-Sung 1997 *Phys. Rev.* B **55** 7904
[30] Yang Z X and Wu R Q 2000 *Surf. Sci.* **447** 212
Yang Z X and Wu R Q 2001 *Phys. Rev.* B **63** 064413
Yang Z X and Wu R Q 2002 *Surf. Sci.* **496** L23
[31] Linder J, Poulopoulos P, Wilhelm F, Farle M and Babersche K 2000 *Phys. Rev.* B **62** 10431
[32] Chen L J, Wu R Q and Freeman A J 1997 *J. Appl. Phys.* **81** 4417
[33] Uiberacker C, Zabloudil J, Weinberger P, Szunyogh L and Sommers C 1999 *Phys. Rev. Lett.* **82** 1289
[34] This accuracy should be viewed cautiously, however, since many factors may worsen the results. It is also important to note that the gradient corrections in the density functional formulism can sometimes alter E_{MCA} very significantly. For example, with a fixed geometry for Co/Cu(001), LDA and GGA gave -0.36 and -0.64 meV/adatom, respectively; cf
Gavrilenko V I and Wu R Q 2000 *J. Appl. Phys.* **87** 6098
[35] Clark A E, Wun-Fogle M, Restorff J B, Lograsso T A, Ross A R and Schlagel D L *Proc. Actuator 2000 Conf. (Berlin)*
[36] Cullen J R, Clark A E, Wun-Fogle M, Restor J B and Lograsso T A 2001 *J. Magn. Magn. Mater.* **226–230** 948
[37] Wu R Q 2002 *J. Appl. Phys.* **91** 7358
[38] Baibich M N, Broto J M, Fert A, Nguyen Van Dau F, Petroff F, Etienne P, Creuzet G, Friedrich A and Chalezas J 1988 *Phys. Rev. Lett.* **61** 2472
[39] Binasch G, Grünberg P, Saurenbach F and Zinn W 1989 *Phys. Rev.* B **39** 4828
[40] Pierce D T, Unguris J, Celotta R J and Stiles M D 1999 *J. Magn. Magn. Mater.* **200** 290
[41] Grünberg P, Schreiber R, Pang Y, Brodsky M B and Sowers C H 1986 *Phys. Rev. Lett.* **57** 2442
[42] Parkin S S P, More N and Roche K P 1990 *Phys. Rev. Lett.* **64** 2304
[43] Ustinov V V, Bebenin N G, Romashev L N, Minin V I, Milyaev M A, Del A R and Semerikov A V 1996 *Phys. Rev.* B **54** 15958
[44] Qiu Z Q and Bader S D 1999 *J. Magn. Magn. Mater.* **200** 664
[45] Uran S, Grimsditch M, Fullerton E E and Bader S D 1998 *Phys. Rev.* B **57** 2705